Leeside Flows over Delta Wings at Supersonic Speeds

David S. Miller* and Richard M. Wood*
NASA Langley Research Center, Hampton, Virginia

Pressure data and three types of flow-visualization data (oil flow, tuft, and vapor screen) were obtained at Mach numbers from 1.7 to 2.8 for wing leading-edge sweep angles from 52.5 to 75 deg. From the flow-visualization data, the leeside flows were classified into seven distinct types depending on the particular flow mechanism observed; e.g., shock or shockless, attached or separated, etc. A chart was developed defining the flow mechanism as a function of the conditions normal to the wing leading edge, specifically, angle of attack and Mach number. Leeside wing pressure data obtained both experimentally and by a semiempirical prediction method were employed to investigate the effects of angle of attack, leading-edge sweep, and Mach number on vortex strength and vortex position. In general, the prdicted and measured values of vortex-induced normal force and vortex position have the same trends with angle of attack, Mach number, and leading-edge sweep; however, the vortex-induced normal force is underpredicted by 15-30% and the vortex spanwise location is overpredicted by approximately 15%.

Nomenclature

c_p = pressure coefficient
$c_{p,v}$ = vacuum pressure coefficient, $= -2/\gamma M^2$
M = Mach number
M_N = component of Mach number normal to the leading edge, $= M\cos\Lambda_{LE}(1+\sin^2\alpha\tan^2\Lambda_{LE})^{1/2}$
α = angle of attack
α_N = angle of attack normal to the leading edge, $= \tan^{-1}(\tan\alpha/\cos\Lambda_{LE})$
β $= \sqrt{M^2-1}$
Λ_{LE} = wing leading-edge sweep angle
η = fraction of local wing semispan
η_v = semispan location of vortex action point

Introduction

DURING the last 20 years aerodynamicists have attempted to design aircraft wings for efficient supersonic flight using attached-flow concepts. For cruise levels of lift, linearized-theory wing-design methods[1,2] have successfully produced optimum twisted and cambered wings. Because of the early success of these methods, the methods have been modified and refined continuously to include the effects of component-on-wing interference,[3] real-flow constraints,[4] and attainable leading-edge thrust.[5] Example applications of this low-level-of-lift wing-design technology can be found in Refs. 6-8.

For maneuver levels of lift at supersonic speeds, basically two approaches are available for the design of wings. One approach is to provide an attached-flow controlled expansion around the wing leading edge and on the upper surface. This attached-flow approach for producing efficient high lift depends on the ability to accelerate the flow around the leading edge to supercritical conditions on the upper surface and then decelerate the flow without causing separation or producing strong shocks; this high-lift, attached-flow wing-design concept has been verified experimentally and a summary of the investigation is given in Ref. 9. The second approach for obtaining efficient high-lift wings uses a controlled, separated, leading-edge vortex flow which not only produces vortex lift, but when the vortex is located on the proper leading-edge shape, also produces significant levels of effective leading-edge thrust. Investigations at subsonic and transonic speeds of the fundamental vortex behavior on the leeward surface of wings have led to the design of several unique and novel leading-edge devices commonly referred to as "vortex flaps." Also, to aid in the design of vortex flaps, several computer codes with varying degrees of complexity are being developed to predict vortex location, strength, and effect on the wing. As summarized in Ref. 10, the development of this new wing-design technology has been extensive but has been confined mainly to subsonic and transonic flows.

The purpose of this paper is to present some fundamental vortex-flow results obtained at supersonic speeds. An experimental investigation was performed in which pressure data and several types of flow-visualization data were obtained on the leeward surface of a series of flat delta-wing models to identify the various flow mechanisms which can occur, and to determine the effect of leading-edge sweep, Mach number, and angle of attack on the vortex strength and location. These results are the first of an investigation to explore the use of wing leading-edge vortex technology as a supersonic wing-design tool.

Discussion

In supersonic flow it is well known that at most moderate angles of attack an uncambered wing with a highly swept (subsonic) sharp leading edge will develop separated flow on the leeside which results in a classical leading-edge vortex. Although most supersonic wing designs try to avoid flow separation, the leading-edge vortex has lift-producing characteristics which could possibly be integrated into a supersonic wing design. The basic leading-edge vortex characteristics are shown in Fig. 1. The figure illustrates a typical spanwise pressure distribution and a sketch of the spanwise flow produced by a classical leading-edge vortex. As shown in the sketch, when the flow attempts to expand around a sharp leading edge, it separates and forms a region of rotational flow referred to as the "primary vortex." The highly rotational primary vortex induces surface velocities which can decrease the wing-pressure distribution relative to the attached-flow pressure distribution (see Fig. 1), and

Presented as Paper 83-1816 at the AIAA Applied Aerodynamics Conference, Danvers, Mass., July 13-15, 1983; received Oct. 25, 1983; revision received March 29, 1984. This paper is declared a work of the U.S. Government and therefore is in the public domain.

*Aero-Space Technologist, Supersonic Aerodynamics Branch. Member AIAA.

produce vortex lift In the classical situation, the primary vortex is above the wing and induces flow which reattaches at a point where there is streamwise flow on the inboard side of this point and outward spanwise flow on the outboard side The outward spanwise flow can separate into a secondary vortex and create additional vortex lift as illustrated by the shaded area in the pressure distribution It is easily seen that if a vortex of sufficient strength could be located on a forward facing surface, the very desirable results of positive lift and negative drag (effective thrust) would be created Although the forward facing surface is a necessary ingredient in the concept, it seems more appropriate to first investigate the effects of leading edge sweep, Mach number and angle of attack on the flow over the more fundamental geometry of an uncambered wing.

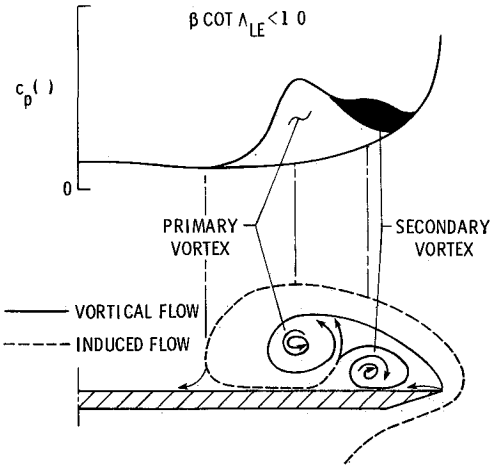

Fig 1 Classical leading edge vortex characteristics

Experimental Test

Five wind tunnel models were selected for testing The models had delta wing planform and leading edge sweep values of 52 5, 60 0, 67.5, and 75 0 deg In this initial test it was desirable to minimize the effect of airfoil shape and thickness; therefore, the leading edge was made sharp (10 deg angle normal to leading edge located on lower surface) and the upper surface was flat. Each model had a span of 12 in and a spanwise row of 19 evenly spaced pressure orifices located approximately 1 in forward of the trailing edge

Previous experimental tests employed only a single type of flow visualization information with or without pressure data to explain the vortex phenomena; however, in this experiment, pressure data were obtained along with three types of flow visualization information Both tuft and oil flow photographs were used to examine the flow characteristics on the model surface and a vapor screen flow visualization technique was used to examine the flowfield above the wing. The surface flow is determined by the angle of the tufts or the streaking of the oil; however, the tufts tend to reflect the velocity direction at the edge of the boundary layer, and the direction of oil streaking is influenced not only by the surface velocity but also by the pressure distribution.

The vapor screen flow visualization technique provides flowfield information on the size, shape, and location of the vortex The dark areas in the vapor screen photographs indicate regions having less vapor than the light regions; thus,

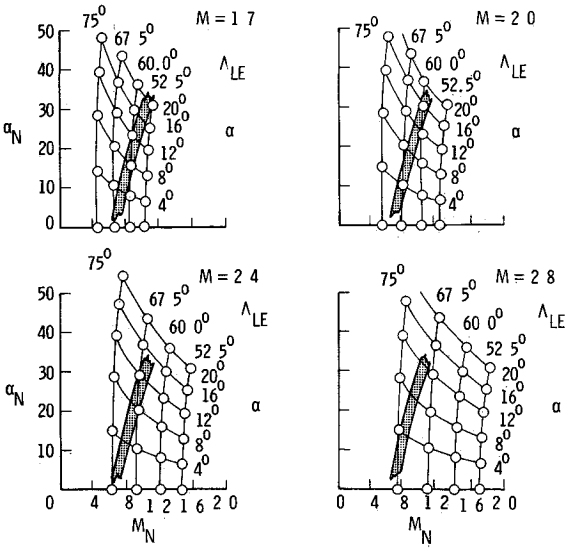

Fig 2 Matrix of test conditions

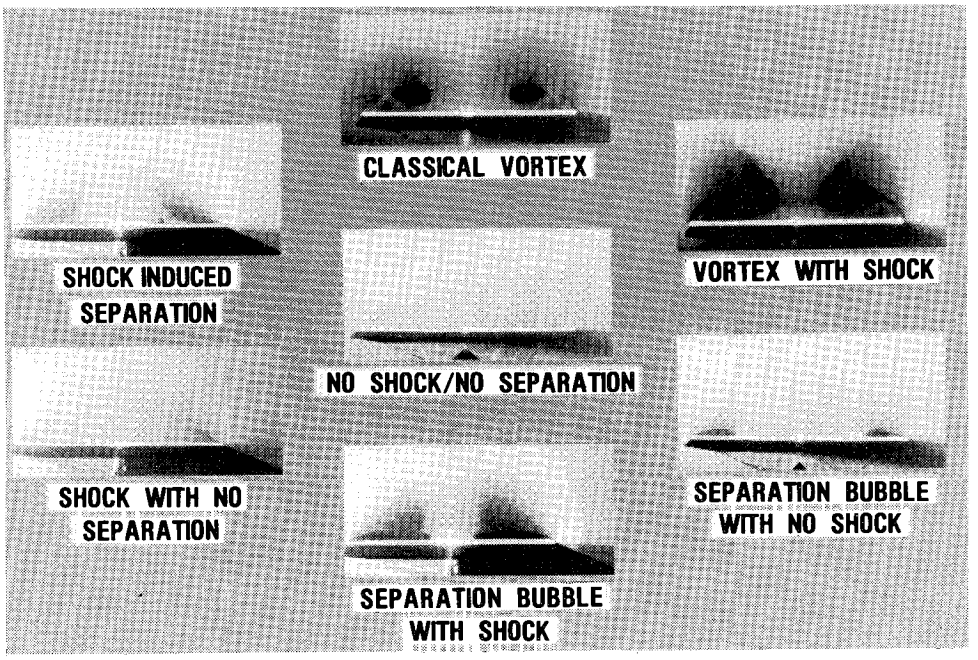

Fig 3 Flow classifications

the dark regions correspond to the highly rotational flow regions in which the vapor particles have been displaced Examples and discussion of interpreting these various types of data and their relationship with leading edge vortex behavior will be given later in this paper

Each model was tested at Mach numbers of 1 7, 2 0, 2 4, and 2 8 for angles of attack from 4 to 20 deg The matrix of test data points of the present study is presented in Fig 2 as a function of conditions measured normal to the wing leading edge, specifically, normal angle of attack (α_N) and normal Mach number (M_N) In a previous study, Stanbrook and Squire[11] reported that near $M_N = 1$, a boundary existed (shaded region in Fig 2), dividing the flow into two distinct regions: to the left of the boundary the flow was characterized by a leading edge, separated, rolled up vortex type flow; and to the right by an attached flow with possible shock induced separation The classification into just two types of flow provided by the Stanbrook Squire boundary was revised by Ganzer et al [12]; however, this latter effort was based on a single leading edge sweep of 73 deg and flow conditions which either coincide with or lie to the right of the Stanbrook Squire separation boundary

Flow Classifications

Through experimental observations of primarily vapor-screen information, the flow has been clearly divided into seven categories as shown in Fig 3 This classification procedure would not have been possible with only oil flow, tuft, and pressure data Except for the no shock/no separation flow, the other six types of flow are discussed with the aid of Figs 4 9 Each figure shows a sketch of oil flow, tuft, vapor screen and pressure data which are typically associated with a particular type of flow

The classical vortex of Fig 4 is characterized by a primary and secondary vortex with no shock The oil flow and tuft patterns are similar in that they both exhibit streamwise flow between the wing centerline and the primary vortex reat tachment line which divides this inboard region of streamwise flow and the adjacent region of primary vortex induced, outward-spanwise flow Both surface flow visualization techniques also distinctly show the second vortex separation line which is the outboard boundary for the primary vortex induced flow region The oil flow data indicate the position of the secondary vortex by an oil accumulation line nearest the wing leading edge This third boundary is not found in the tuft data The pressure distribution shows the significant negative pressures induced by the vortex

For large values of angle of attack, the vortex with shock situation shown in Fig 5 is a common occurrence for both subsonic and supersonic leading edges In this flow class, the shock is located on top of the vortex and the presence of the shock is not indicated in either the oil-flow or tuft patterns The general flow pattern of the vortex with shock is similar to the classical vortex surface flow pattern of Fig 4 when shifted inboard, and the inboard streamwise flow of Fig 4 is no longer present in Fig 5 Apparently, the effect of the shock is limited to the flow region above and external to the vortex and, therefore, no shock effects are indicated in either the surface flow patterns or surface pressure distributions

Figure 6 shows typical results for a leading edge separation bubble with no shock In contrast to the vortex, a separation bubble is defined as having its entire rotational flow contained within its boundaries and exhibits no secondary separation Except for a small amount of oil accumulation along the leading edge, the oil flow and tuft photographs exhibit only two distinct flow patterns; streamwise flow inboard and spanwise flow outboard, where the dividing line corresponds to the termination of the separation bubble Thus, the effects of the separation bubble are much more confined to the

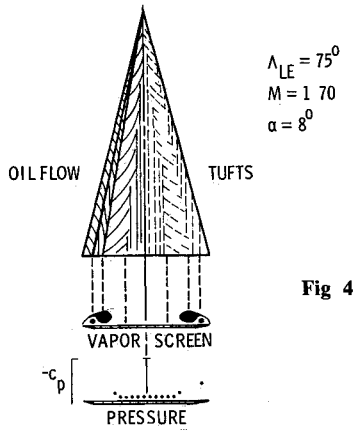

Fig 4 Classical vortex

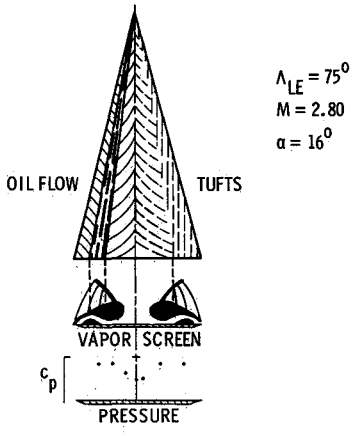

Fig 5 Vortex with shock

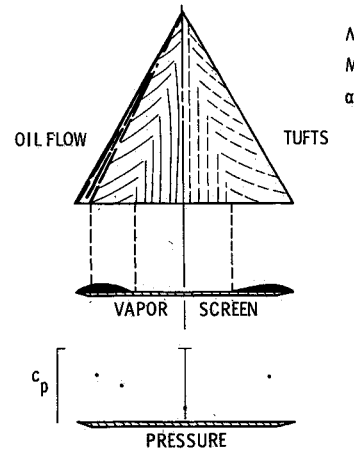

Fig 6 Separation bubble with no shock

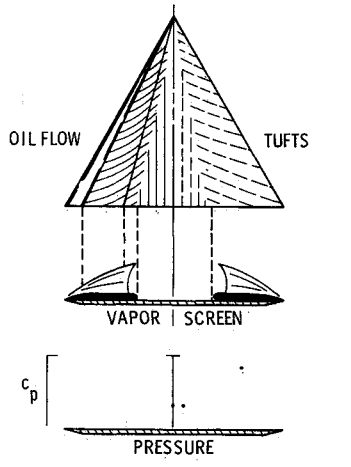

Fig 7 Separation bubble with shock

leading edge than those of the classical vortex, and the pressure distribution reflects a considerable amount of lifting pressure augmentation

As in the case of the vortex the situation can occur where the separation bubble develops a shock located on top as shown in Fig 7 The tuft flow pattern of Fig 7 is identical to that in Fig 6 with no indication that a shock has developed; however, the oil flow pattern of the two figures is distinctly different with an obvious oil accumulation line present in the vicinity of the shock Unlike the vortex with shock situation the effect of the shock on top of the bubble is clearly evident in both the oil flow patterns and the surface pressures. The shock is distinguished in the oil flow pattern by an oil accumulation line located within the bubble induced span wise flow region and in the surface pressures by the large pressure gradient

For sharp leading edge wings the last two types of flow occur for supersonic leading edge conditions only For both types, the flow on and immediately behind the leading edge is attached and directed inboard until a shock is encountered as shown in the vapor screen data of Figs 8 and 9 If the shock is weak it simply deflects the flow downstream with no separation (see Fig 8); however, if the shock is strong, it induces separation in the form of a separation bubble located immediately inboard of the shock (see Fig 9) In both types of flow, it is very difficult to detect a shock from the oil flow or tuft patterns, and the vapor screen data were the principal means of detecting shocks However, the tufts tend to flutter at the shock location and this fluttering appears as random wiggles in the tuft flow patterns of the types shown in Fig 8 Without vapor screen data, and except for the fluttering of the tufts at the shock location, the oil flow and tuft patterns of Fig 8 could be misinterpreted as shockless attached flow, and the patterns of Fig 9 could be misinterpreted as the classical vortex flow of Fig 4

In order to summarize all of the test data according to flow type, each of the test conditions shown in Fig 2 was classified according to one of these seven flow types and the results are shown in Fig 10 The α_N-M_N space is clearly divided into regions where the flow type is indicated by the vapor screen sketch placed in each region As an added feature to provide additional information, flows with or without shocks are denoted by open or closed symbols, respectively Also, the symbol shape is used to identify the character of the rotational flow where the circular symbols denote flows with primary and secondary vortices, and the square symbols denote flows containing separation bubbles As shown by the solid triangles in the figure, the only flow conditions which produced shockless attached flows were angles of attack of zero ($\alpha_N = 0$); however, this may have occurred because the next smallest angle of attack in the test matrix was 4 deg The results of Fig 10 can be used to interpret oil flow or tuft patterns where there is some question about the flow type; for example, the tuft-flow pattern of Fig 9 should not be mistakenly identified as a classical vortex because the con ditions of $\Lambda_{LE} = 60$ $M = 2\ 8$, and $\alpha = 8$ deg correspond to $M_N = 1\ 4$ and $\alpha_N = 15\ 7$ deg which lies in the shock induced separation region of Fig 10. Because the two most effective types of separated flow being considered for performance enhancements are the shockless bubble and shockless vortex, it is interesting to note that these two types of flow occupy the majority of the region for M_N less than unity Also above 20 deg normal angle of attack, the upper boundary of the region decreases toward M_N of zero with increasing α_N

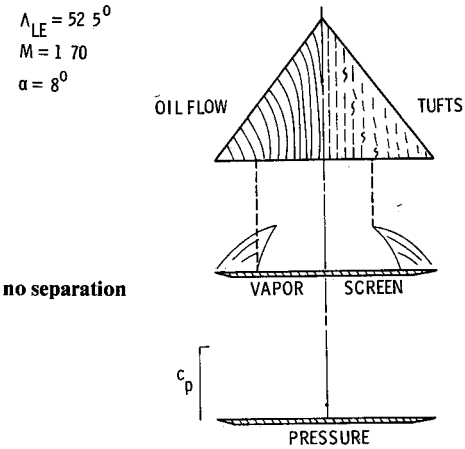

Fig 8 Shock with no separation

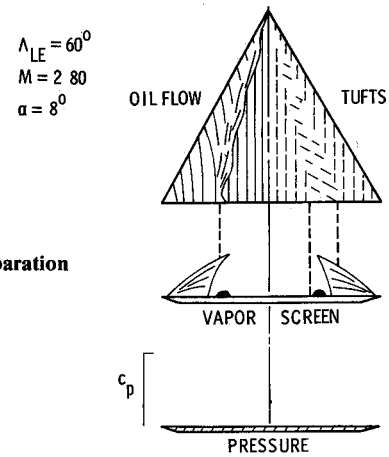

Fig 9 Shock induced separation

Vortex Strength and Location

In the development of vortex flap technology, the flap loads and moments and thus vortex strength and position are very important. Aerodynamically, the vortex strength and location are important because it is desirable to maximize effectiveness through the selection of wing planform flap planform, and flap deflection Structurally, loads and moments are required for the selection and sizing of the actuator mechanism Thus, it is necessary to understand the behavior of the vortex flow, and specifically to know how the vortex strength and location vary with wing flap shape and flow conditions For the present delta wing study, the only wing shape parameter is the leading edge sweep, Λ_{LE} The flow condition parameters are simply Mach number and angle of attack In the remainder of this paper, the effect of leading edge sweep Mach number and angle of attack on the vortex strength and location will be discussed

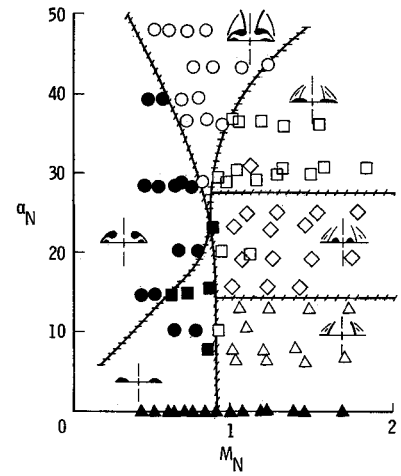

Fig. 10 Classification of test data

The vortex strength and location information was extracted from the measured and predicted upper surface spanwise pressures, as illustrated in Fig 11 The theoretical pressures are predicted using a computational method[13] which produces both attached flow ("theory without vortex") and separated flow ("theory with vortex") values The attached flow is represented by linearized theory which has been modified to account for attached flow nonlinearities occurring on wings at large angles of attack; the separated flow is represented by a semiempirical technique which uses the Polhamus suction analogy to determine the leading edge vortex force and then modifies the upper surface attached flow pressures to distribute this additional force over the wing upper surface For the purpose of examining the vortex strength, the two theoretical and one experimental spanwise pressure distributions have been integrated across the span to yield a section normal force parameter,

$$\int_0^1 (c_p/c_{p\,v})\,d\eta$$

The vortex strength then can be examined in terms of dif ferences in this normal-force parameter for variations in leading edge sweep, Mach number, and angle of attack The vortex location can be defined in terms of its position in space; however, in this study, the vortex location is defined as the point on the wing at which the normal force vector should be placed to give the same moment as the vortex induced pressure distribution This latter definition is referred to as the "vortex action point," η_v, and the method for computing it from the upper surface pressures is shown in Fig 11 As shown in Fig 12, a range of planform and flow condition parameters was selected to encompass the entire region designated to exhibit the classical vortex type flow For each variation of a given parameter, the other two parameters were held constant, e g , for the α variation, the Mach number and leading edge sweep had values of 1 7 and 75, deg respectively Results for other combinations of parameters were examined are those presented here and considered typical

The effect of angle of attack on vortex strength is shown in Fig 13 For three angles of attack inset sketches of the pressure distributions used to obtain the normal force parameter are also shown in the figure The difference be tween the theory without vortex values and either ex perimental or theory with vortex values represents, respec tively, the experimental or theoretical vortex induced normal force increment For the entire angle of attack range the vortex accounts for approximately a 50% increase in the attached flow normal force In terms of the vortex force increment, the theory underpredicts the experimental values by about 30%, except at the largest value of α where the difference is less than 15% The pressure distributions in dicate that at the lower three fourths of the angle of attack range, the theory predicts nearly the correct pressure distribution shape, but, as reflected in the normal force underpredicts the level At the larger α, where the normal force agreement is best, the theory predicts both the shape and level of the pressure distribution incorrectly

In Fig 14 it can be seen that the section normal force parameter increases at a slightly decreasing rate with Mach number and this trend with Mach number is predicted by the theory The experimental vortex normal force increment has a constant value of 0 125, which apparently does not vary with Mach number; however, the theoretically predicted increment is 30 50% less than the experimental value The correspon ding spanwise pressure distributions are also shown in the figure; the most outstanding observation is that the theory tends to underpredict the pressure parameter, $c_p/c_{p\,v}$, in the vortex-affected region regardless of Mach number. The theory also tends to overpredict the pressure parameter in the inboard attached flow region and this overprediction becomes more pronounced with increasing Mach number.

The effect of leading edge sweep on vortex strength can be deduced by the normal force parameter variations shown in Fig 15 The two theoretical curves are coincident up to a Λ_{LE} value of 60 deg at which point they depart at an increasing rate with leading edge sweep; this is due to the absence of any theoretical vortex force below 60 deg However, it appears that the experimental normal force and pressure distributions indicate that a small amount of experimental vortex force may

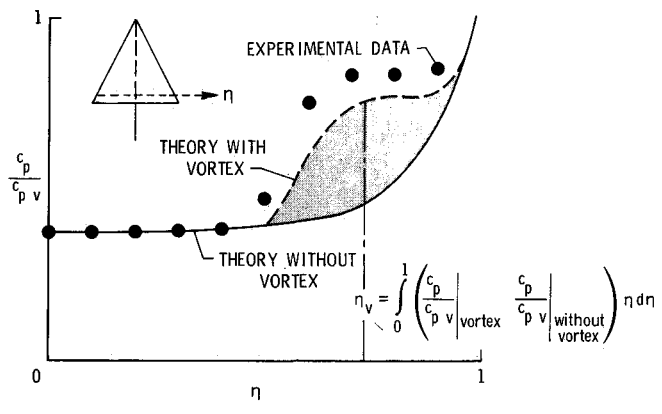

Fig 11 Typical spanwise upper surface pressure distributions

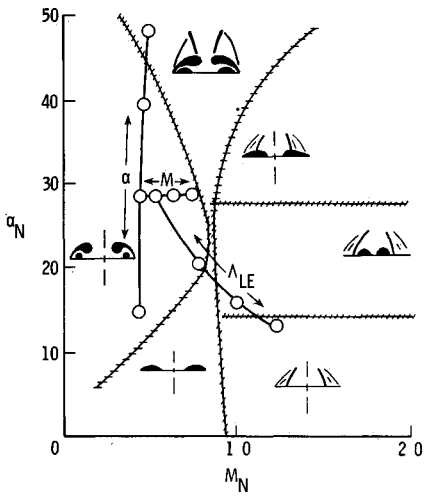

Fig 12 Variation of $\alpha\Lambda_{LE}$, and M for parametric study

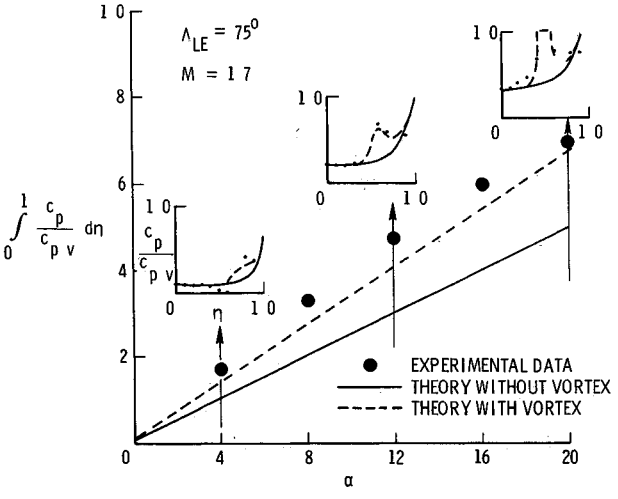

Fig 13 Effect of angle of attack on vortex strength

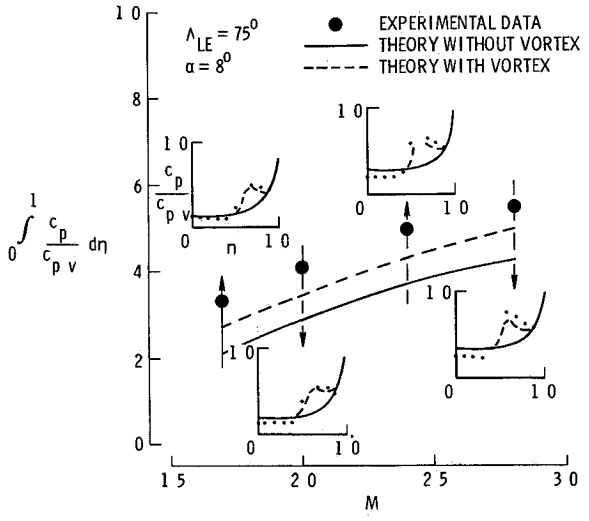

Fig. 14 Effect of Mach number on vortex strength

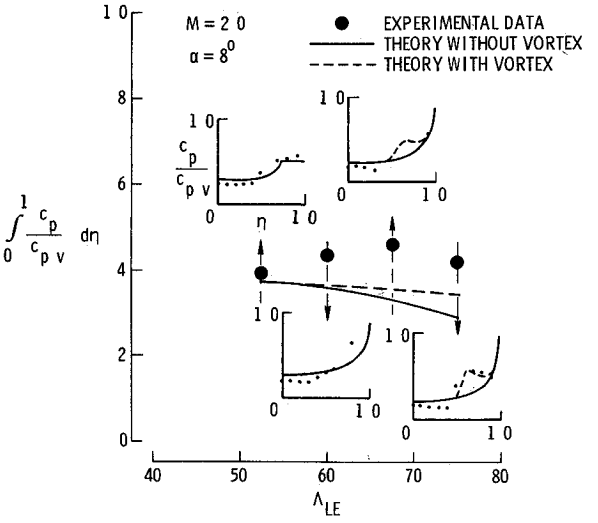

Fig 15 Effect of leading edge sweep angle on vortex strength

exist even at the smallest leading edge sweep value and the vortex force increases with increasing leading edge sweep From the location of the smallest two values in Fig 12 it is clearly possible that a shock induced separation bubble could exist which is responsible for the larger experimental normal force shown in Fig 15

The effects of angle of attack, Mach number, and leading edge sweep on the vortex position are shown in Fig 16. As shown in the sketch, the vortex position is identified by the location of the vortex action point which is expressed on the figure as the fraction of the local wing span, η_v The vortex action point is the semispan position at which the vortex normal force vector should be placed to give the same moment as produced by the vortex induced pressures The theoretical value shown was computed from the method of Ref 13 which is an empirical formulation and, as shown in the figure, is only a function of the angle of attack The experimental value was obtained using the expression given in Fig 11 where the vortex $c_p/c_{p,v}$ values correspond to the experimental data As indicated by both experimental and theoretical results, the most pronounced change occurs for the inboard movement of the vortex location with increasing angle of attack Typically, the vortex action point moves from a location near 80% span to a location near 50% span as

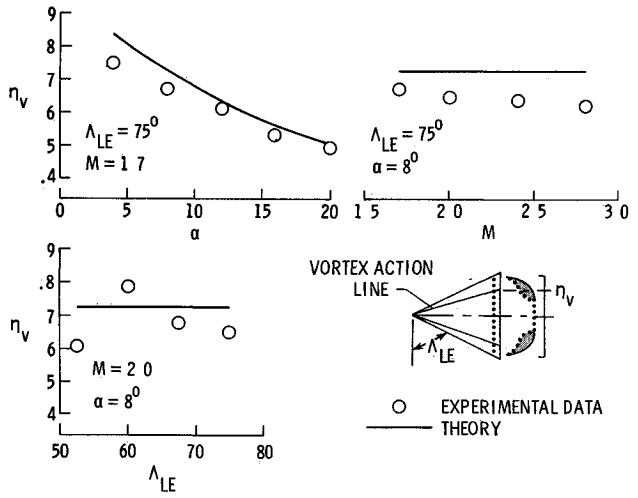

Fig 16 Location of vortex action line

angle of attack changes from 4 to 20 deg According to the method of Ref 13, there is no change in the vortex action point with either Mach number or leading edge sweep Experimentally, only a very small inboard movement was observed with increased Mach number, and a small but inconsistent variation was observed with change in leading edge sweep In general, the experimental vortex location is usually inboard of the theoretically predicted location and the two values agree within 15%

Concluding Remarks

An experimental investigation of the upper surface flow on sharp leading edge delta wings at supersonic speeds has been conducted Pressure data and three types of flow visualization data (oil flow, turft, and vapor screen) were obtained at Mach numbers from 1 7 to 2 8 for wing leading edge sweep angles from 52.5 to 75 deg

From the flow visualization data, the upper surface flows were classified into seven distinct types depending on the particular flow mechanism observed; e g , shock or shockless, attached or separated, etc A chart is presented which defines the flow mechanism as a function of the conditions normal to the wing leading edge, specifically, angle of attack and Mach number

Measured and predicted upper surface wing pressure data were employed to investigate the effects of angle of attack, leading edge sweep angle, and Mach number on vortex strength and vortex position In general, the vortex induces an incremental normal force which, in some cases, was found to increase the attached flow normal force (upper surface contribution) by as much as 50% The location of the vortex action point was found to be most sensitive to variations in angle of attack; in general, the action point moves from 80 to 50% of the local span as the angle of attack changes from 4 to 20 deg As the action point moves inboard according to the method of Ref 13, a larger portion of the vortex influence region moves off the wing and becomes ineffective in producing normal force. This may explain why the experimentally measured vortex induced normal force increases linearly with angle of attack and not quadratically according to the full-suction analogy; the full suction analogy which assumes that the entire vortex influence region is not distributed but is concentrated at the wing leading edge

Experimental results were compared with results of one semiempirical prediction method. In general, the predicted and measured values of normal force and vortex location have the same trends with α M and Λ_{LE}; however, the vortex normal force is underpredicted by 15 30% and the vortex location is overpredicted by approximately 15%

References

[1]Carlson H W and Middleton, W D A Numerical Method for the Design of Camber Surfaces of Supersonic Wings with Arbitrary Planforms ' NASA TN D 2341 1964

[2]Carlson H W and Miller D S Numerical Methods for the Design and Analysis of Wings at Supersonic Speeds NASA TN D 7713 1974

[3]Mack R. J ' A Numerical Method for Evaluation and Utilization of Supersonic Nacelle Wing Interference NASA TN D 5057, March 1969

[4]Kulfan R M and Sigalla A Real Flow Limitations in Supersonic Airplane Design " AIAA Paper 78 147, Jan 1978

[5]Carlson H W and Miller D S , The Influence of Leading Edge Thrust on Twisted and Cambered Wing Design for Supersonic Cruise AIAA Paper 81 1656 Aug 1981

[6]Carlson H W Aerodynamic Characteristics at Mach Number 2 05 of a Series of Highly Swept Arrow Wings Employing Various Degress of Twist and Camber ' NASA TM X 332 1960

[7]Morris O A and Fournier R H , Aerodynamic Characteristics at Mach Numbers 2 30 2 60 and 2 96 of a Supersonic Transport Model Having a Fixed, Warped Wing NASA TM X 1115 1965

[8]Miller D S and Schemensky R T Design Study Results of a Supersonic Cruise Fighter Wing ' AIAA Paper 79 0062 Jan 1979

[9]Miller D S Pittman J. L and Wood, R M , An Overview of Two Non-Linear Supersonic Wing Design Studies ' AIAA Paper 83 0182 Jan 1983

[10]Lamar J E and Campbell J F Recent Studies at NASA Langley of Vortical Flows Interacting with Neighboring Surfaces Paper 10 AGARD Symposium on Vortical Type Flows in Three Dimensions Rotterdam Netherlands, 1983

[11]Stanbrook A and Squire L C , Possible Types of Flow at Swept Leading Edges *Aeronautical Quarterly* Vol XV Feb 1964 pp 72 82

[12]Ganzer W Hoder H and Szodruch J , On the Aerodynamics of Hypersonic Cruise Vehicles of Off Design Con ditions *Proceedings of the XI Congress of the ICAS* Lisbon Portugal Vol I Sept 1978 pp 152 161

[13]Carlson H W and Mack R J Estimation of Wing Nonlinear Aerodynamic Characteristics at Supersonic Speeds NASA TP 1718 1980